

An Efficient Gain Estimation in the Calibration of Noise-Adding Total Power Radiometers for Radiometric Resolution Improvement

S. Bonafoni[✉], Member, IEEE, F. Alimenti, Senior Member, IEEE, and L. Roselli, Fellow, IEEE

Abstract—Calibration of microwave radiometers is a crucial task for reliable and accurate antenna temperature measurements in remote sensing applications. This paper describes a processing procedure for data calibration of noise-adding (NA) total power (TP) radiometers, without thermal stabilization, able to improve the radiometric resolution performance and keep good accuracy. This method, easily implementable, is based on the strong dependence of the radiometric gain on the internal physical temperature of the system. It provides a calibration of the output voltage measured in the TP mode exploiting the noise source power injection only every 30 min. The quality of the proposed procedure was assessed by means of three experiments carried out in different years and environmental conditions, using a low-cost NA TP radiometer operating at 12.65 GHz. The measurements show an uncertainty better than 0.7 K and, above all, a clear improvement in radiometric resolution (below 0.1 K). The radiometric resolution benefit is particularly appreciable in applications where the aim is the detection of small radiation power increments. Two experimental tests show how this method for data calibration effectively resolves the warm target counting inside the antenna footprint, while the same data measured with the standard NA procedure do not allow the same detection capability.

Index Terms—Calibration, noise adding, radiometric gain, radiometric resolution, total power (TP) radiometer.

I. INTRODUCTION

THE microwave radiometers represent a powerful tool for the remote sensing of different scenarios, from earth observation to indoor applications. The use of ground-based microwave radiometers for remote sensing outdoor applications is well known: a typical use is for the retrieval of constituents and physical parameters of the atmosphere (temperature and humidity profiles, precipitable water vapor, and cloud liquid) and for the estimation of land parameters (soil moisture, sea surface salinity and temperature, and vegetation parameters) [1]–[4]. For instance, a ground-based radiometer operating around 13 GHz (the same frequency of the instrument used in this paper) can be used for long-term recording of propagation conditions and atmospheric attenuation observations, test measurements of satellite communication payloads, and for rainy-cloud parameter retrieval [5], [6].

Manuscript received December 5, 2017; revised February 20, 2018; accepted March 2, 2018. Date of publication March 22, 2018; date of current version August 27, 2018. (*Corresponding author: S. Bonafoni.*)

The authors are with the Department of Engineering, University of Perugia, 06125 Perugia, Italy (e-mail: stefania.bonafoni@unipg.it).

Color versions of one or more of the figures in this paper are available online at <http://ieeexplore.ieee.org>.

Digital Object Identifier 10.1109/TGRS.2018.2812904

In addition, further outdoor applications are possible with a microwave radiometer (fire detection in different scenarios [7], [8], subsurface sensing [9], [10]) as well as indoor applications (detection of small warm targets [11], sensing of building interiors [12]).

For each application, the radiometric resolution (minimum change at the radiometer input that can be detected by the output, determined by the standard deviation of the system input noise temperature) and the absolute accuracy (correspondence between actual and measured values, depending chiefly on the accuracy of the calibration) are the two main radiometer attributes required for reliable measurement processes [1]. The radiometer calibration consists of finding parameters relating the receiver output voltage to the antenna noise temperature at the input.

Different types of radiometric schemes can be adopted (in microwave remote sensing the total power (TP) radiometer is commonly used as basic scheme), as well as different calibration approaches and related circuitry [1], [13]. Although the TP radiometer scheme is simple, its calibration is a crucial and challenging task affected by physical temperature variations, aging of system components and relevant fluctuations of the electrical properties.

Over the years, several efforts have been made to adopt calibration solutions counteracting the component drifts. For example, the use of a switching mechanism is a well-known procedure, even if handling the calibration by switched-type radiometers [1], [13], [14] has the drawback of greater complexity and higher costs. Radiometers can adopt thermal stabilization to keep constant the system component parameters sensitive to physical temperature variations, but, again, extra cumbersome hardware and power are necessary [2], [15].

In applications demanding low-cost systems with limited power consumption, the noise-adding (NA) TP radiometer without thermal stabilization can be a good solution, combining the benefit of the lower complexity of a TP scheme with the efficiency of the NA calibration technique able to correct parameter variations due to temperature drifts.

A continuous NA calibration, however, causes a decrease of the radiometric resolution with respect to that achievable with the same receiver operating in TP mode. In this paper, to avoid such a radiometric resolution degradation, we propose an approach for the calibration data processing, specifically designed for the case of absence of thermal stabilization. The basic idea is to adopt a temperature compensation procedure

0196-2892 © 2018 IEEE. Personal use is permitted, but republication/redistribution requires IEEE permission.
See http://www.ieee.org/publications_standards/publications/rights/index.html for more information.

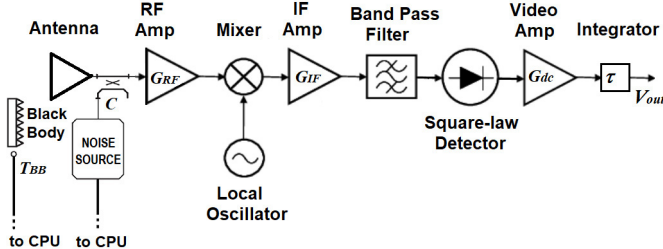


Fig. 1. Block diagram of a TP radiometer with NA mechanism.

for the calibration gain estimation between two selected NA injections. In such a way, the radiometer can be used in TP mode, i.e., with better radiometric resolution, by reducing significantly the NA injections. To this extent, we explore a combination between calibration and compensation techniques for a NA radiometer. This method has also been compared with the physical temperature compensation method suggested in the literature to calibrate a TP radiometer [16]–[18].

We tested the proposed strategy using antenna temperatures provided by a low-cost NA TP radiometer, without thermal stabilization, operating at 12.65 GHz. Three experiments (one outdoor and two indoor) were carried out: the first, with a blackbody target, allowed the method accuracy and radiometric resolution to be assessed in different environmental conditions; the other two ones allowed the method capability to detect small radiation increment not clearly distinguishable with the standard NA mode to be evaluated.

II. NOISE-ADDING TOTAL POWER RADIOMETER OVERVIEW

The NA TP radiometer is an enhanced version of the classical TP one where the NA circuitry removes the effects of gain variations without the use of any switch system [1], as in the Dicke radiometer [14]. The noise source is used to inject a known amount of noise power into the receiver input. A typical block diagram is reported in Fig. 1. Examples of noise sources are reported in [19]–[21]. The absence of an input switch is a key feature, since expensive and lossy devices are avoided.

The basic theory of the NA radiometer is well known [1], [13]: in the following, since the instrument function is to measure the scenario radiation power delivered by the antenna to the receiver, the key equations are reported to describe the retrieval of the antenna temperature T_A .

When the calibration noise source is switched OFF, henceforth referred to as the TP mode, the mean value of the voltage at the radiometer output, V_{OFF} , can be expressed as (Nyquist's law)

$$V_{\text{OFF}} = k_B(T_A + T_R + T_{\text{OFF}})B_{\text{IF}}G_{\text{RF}}G_{\text{IF}}G_{\text{dc}}\gamma + \beta_{\text{dc}}G_{\text{dc}} \quad (1)$$

where k_B is the Boltzmann constant, T_A is the antenna temperature, T_R is the equivalent input noise temperature of the receiver, T_{OFF} is the equivalent noise temperature injected by the noise source into the receiver input port when the source is OFF, B_{IF} is the equivalent noise bandwidth of the system, G_{RF} , G_{IF} , and G_{dc} are the RF, intermediate frequency (IF)

and video gains of the system, respectively, γ is the square-law detector constant, and β_{dc} is the video amplifier offset. If an input directional coupler is used to adjust the injected noise power, $T_{\text{OFF}} = CT_{\text{NS}}$, with C the coupling factor of the directional coupler and T_{NS} the physical temperature of the noise source [7].

When the calibration noise source is switched ON, henceforth referred to as the NA mode, voltage at the radiometer output, V_{ON} , is

$$V_{\text{ON}} = k_B(T_A + T_R + T_{\text{ON}})B_{\text{IF}}G_{\text{RF}}G_{\text{IF}}G_{\text{dc}}\gamma + \beta_{\text{dc}}G_{\text{dc}} \quad (2)$$

where T_{ON} is the equivalent noise temperature injected by the source when it is ON. From the measurements in (1) and (2), the calibration equation in NA mode to retrieve T_A is [16]

$$T_A = GV_{\text{OFF}} - B \quad (3)$$

$$G = A/(V_{\text{ON}} - V_{\text{OFF}}) \quad (4)$$

where G (K/V) is the radiometric gain in NA mode, B (K) is the radiometric offset, A (K) is a calibration constant. The A and B constants depend on the system parameters, as reported in [13].

In the following, we will refer to the low-cost NA TP radiometer (MWR_NA) developed in [7] and [8], operating at 12.65 GHz, the measurements of which, collected in three experiments, will be processed.

For MWR_NA, where the noise injection circuitry is realized with a precision solid-state noise source and a WR75 directional coupler, the constant $A = 87.4$ K was experimentally determined and found in good agreement with its theoretical expression [7].

While the NA mode is adopted continuously to correct for system gain fluctuations, B is periodically determined (every 30 min) by closing the horn antenna on a motorized blackbody, the physical temperature of which, T_{BB} , is acquired simultaneously. Therefore, since the blackbody brightness temperature is equal to T_{BB} , B is computed as

$$B = GV_{\text{OFF}} - T_{BB}. \quad (5)$$

All the other measurement and calibration operations are synchronized and carried out automatically by a microprocessor unit, with an integration time τ that can be fixed in the range between 0.1 and 10 s.

The evaluation of the receiver calibration accuracy was assessed with rigorous tests in [7] and [8]; the radiometric resolution ΔT of MWR_NA was experimentally performed in [7] for T_A around 300 K: in TP mode, a ΔT of 70 mK is obtained for $\tau = 1$ s, which improves to around 50 mK for $\tau = 10$ s. In the NA mode, ΔT rises to 0.4 K for $\tau = 1$ s, in good agreement with the radiometric resolution theory evaluation for nonideal radiometers reported in [1] and summarized in Appendix I.

The acquisition of the two voltages V_{OFF} and V_{ON} determines the measurement cycle duration (i.e., the duty cycle). Once τ has been fixed, a T_A observation is provided every 2.7τ s, since the system performs a data integration for the noise source both switched ON (for τ s) and switched OFF (for τ s), considering also the time integration for the transients in the switching operations.

A key feature of MWR_NA is the absence of thermal insulation and stabilization. The stabilization is usually adopted to hinder the variations of the internal physical temperature to which the radiometric gain is very sensitive [2]. A radiometer without thermal insulation and stabilization avoids active heating or cooling mechanisms, and therefore further costs and power consumption (for MWR_NA it is about 3 W). Consequently, (4) is used to correct for the receiver gain variations due to physical temperature drifts. On the other hand, NA mode causes a decrease of ΔT compared to that achievable with the same receiver operating in TP mode.

Considering the aspects above, the proposed procedure (Section V) for data calibration of a NA TP radiometer without thermal stabilization is designed to get the following main advantages.

- 1) A ΔT improvement exploiting predominantly the TP mode output voltage (as highlighted later, it will be crucial for the detection of targets with small radiation power variations).
- 2) An absolute accuracy similar to the one in standard NA mode.
- 3) A reduction of the integration time reserved for acquisitions in NA mode, and therefore a shorter T_A measurement cycle.

III. EXPERIMENTS

To assess the performance of the proposed method, described in detail in Section V, three experiments were considered. These experiments were carried out during different years and by using a standard horn antenna with beamwidth $\beta = 30^\circ$ and gain of 15 dBi, assumed as ideal. The impact of antenna losses and mismatches on T_A is reported in Appendix II.

Experiment 1: Outdoor experiment lasting six consecutive days (March 15–20, 2008) [8], with the instrument exposed to strong ambient temperature variations. The radiometer antenna was pointed toward a panel covered with microwave absorbing material (unity emissivity). During the six days, the physical temperature of the absorbing material (T_{BB}) was acquired together with the antenna temperature T_A measured by the radiometer itself and with the internal physical temperature of the receiver (T_{PH}). The T_{BB} range was 273–305 K, while the T_{PH} range was 281–315 K. Data integration time τ was 10 s. The radiometer worked both in TP and NA mode: measurements in TP mode have been used to assess the calibration methods analyzed in this paper.

Experiment 2: Indoor experiment of about 6 h (February 2, 2017), with integration time $\tau = 1$ s. The T_{PH} range is 295–300 K. This laboratory test was carried out to assess the capability of a microwave radiometer to detect warm targets having small filling factors [22] inside the antenna footprint. The target was water warmed up and poured in small styrofoam bins: in specific time intervals, they were placed sequentially inside the antenna field of view, as described in detail in [11]. The styrofoam thermally insulated the liquid and has a transmissivity better than 0.99 in the microwave band.

Experiment 3: Indoor experiment of about 1 h and 20 min (February 23, 2017), with integration time $\tau = 1$ s. The T_{PH} range is 298–299 K. It was similar to experiment 2, but with warmed oil instead of water. Between experiments 2 and 3, the radiometer was turned OFF.

Experiment 1 was selected to assess rigorously the method performance for a long time, experiments 2 and 3 chiefly to prove the detection capability of small radiation power increments.

IV. TOTAL POWER MODE: TEMPERATURE COMPENSATION FROM LITERATURE ALGORITHMS

For a better comprehension of the motivation behind the development of our technique, it is useful to report here an evaluation of the accuracy provided by previous methods found in the literature to calibrate total power radiometers without thermal stabilization employing a temperature compensation approach [16]–[18]. The low performance obtained, in fact, was the main motivation for the development of the proposed method.

With reference to Section II, if the system works only in TP mode, V_{OFF} alone is measured and T_A is obtained by simply solving the output voltage equation reported in (1) as

$$T_A = M \cdot V_{OFF} - B \quad (6)$$

$$M = 1/(k_B B_{IF} G_{RF} G_{IF} G_{dc} \gamma). \quad (7)$$

As well known, different sources of instability make the solution of (1) with the above gain M (K/V) and offset B useless for antenna temperature measurements. As explained in Section II, radiometers are usually exposed to environmental temperature variations, and the internal physical temperature of the instrument T_{PH} strongly influences the T_A correctness without an accurate temperature control.

The temperature-compensation method (henceforth TempComp) in [17] and [18] uses the physical temperature T_{PH} to estimate both the gain and the offset of the receiver. Gain M and offset B are expressed as a function of the radiometer internal temperatures T_{PH} as [17]

$$M = m_0 + m_1 T_{PH}; \quad B = b_0 + b_1 T_{PH} + b_2 T_{PH}^2 \quad (8)$$

where m_i and b_i are the compensation coefficients.

The determination of m_i and b_i is obtained by least-squares estimation measuring a target of known brightness temperature at each data point. In particular, the procedure uses the uncalibrated radiometer output voltage V_{OFF} , the internal physical temperature T_{PH} , and the known temperature of a calibration load, e.g., a blackbody, the brightness temperature of which is equal to its physical temperature T_{BB} .

In the three experiments, $T_{PH} = (T_{NS} + T_{LNB})/2$, where T_{LNB} is the physical temperature of the low noise block (LNB). Both T_{NS} and T_{LNB} were continuously measured.

Data in a calibration period (training set) are chosen to find the set of m_i and b_i by the least-squared error method leading to a system of linear functions of m_i and b_i combined with powers of V_{OFF} , T_{PH} , and T_{BB} , as described in [18].

Outside of this characterization period (test set), (6) and (8) are used to retrieve the radiometric output T_A and perform

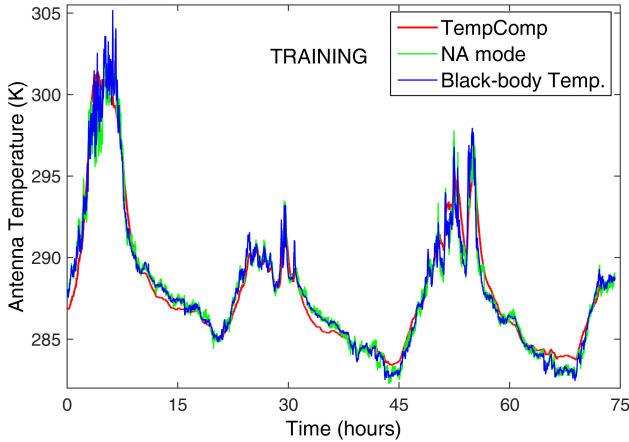


Fig. 2. Experiment 1 (March 15–20, 2008). Training set (first three days): time series of blackbody temperature T_{BB} (blue), T_A measured by the radiometer in NA mode (green), and T_A estimated using the TempComp method (red).

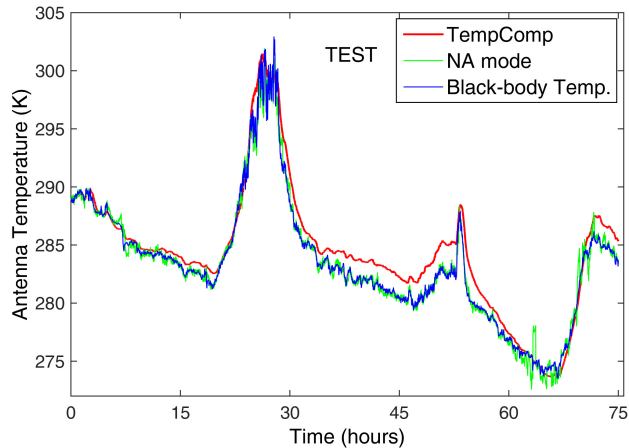


Fig. 3. Experiment 1 (March 15–20, 2008). Test set (last three days): time series of blackbody temperature T_{BB} (blue), T_A in NA mode (green), and T_A estimated using the TempComp method (red).

an assessment of the reliability of m_i and b_i as calibration coefficients using an independent data set, i.e., a set of data different from the training one.

A. TempComp Results

Concerning experiment 1, we consider as training set the first three days and as test-set the last three days. Results are shown in Figs. 2 and 3; the uncertainty of the method in terms of root-mean-square error (RMSE) is reported in Table I.

For experiment 2, the training set consists of the first 3.5 h and the test set of the last 2.5 h. Results are shown in Figs. 4 and 5.

For experiment 3, the training set includes the first 50 min and the test set the last 30 min. Results are shown in Figs. 6 and 7. Table I reports the corresponding RMSE.

In the training phase of experiments 2 and 3, we considered the radiometer output T_A in NA mode as the target for the coefficient computation: experiment 1 has shown how the T_A 's in NA mode are well calibrated in both gain and offset with respect to the T_{BB} . The ramps in Figs. 5–7 are the radiative

TABLE I
RMSE (K) FOR THE THREE EXPERIMENTS USING THE TEMPCOMP METHOD, AND FOR TRAINING SET AND TEST SET

Comparison	Training-set	Test-set
Experiment 1		
T_{BB} vs. T_A NA mode	0.49 K	0.57 K
T_{BB} vs. T_A TempComp	0.86 K	1.41 K
Experiment 2		
T_A NA mode vs. T_A TempComp	0.36 K	1.00 K
Experiment 3		
T_A NA mode vs. T_A TempComp	0.36 K	1.37 K

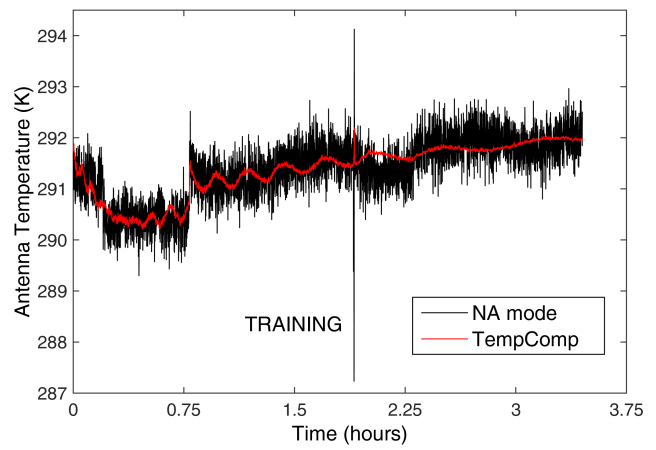


Fig. 4. Experiment 2 (February 2, 2017). Training set (first 3.5 h): time series of T_A measured in NA mode (black) and T_A estimated using the TempComp method (red).

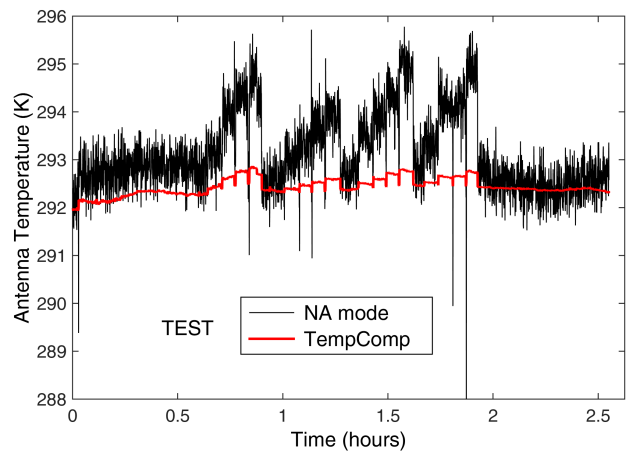


Fig. 5. Experiment 2 (February 2, 2017). Test set (last 2.5 h): time series of T_A in NA mode (black) and T_A estimated using the TempComp method (red).

effects of the hot liquids in small bins placed sequentially inside the antenna beam: details of such bin insertion and their effects are described in Section VI-A.

Even if the T_A estimated by TempComp method is “less noisy,” i.e., for $\tau = 1$ s, $\Delta T = 0.07$ K in TP mode and

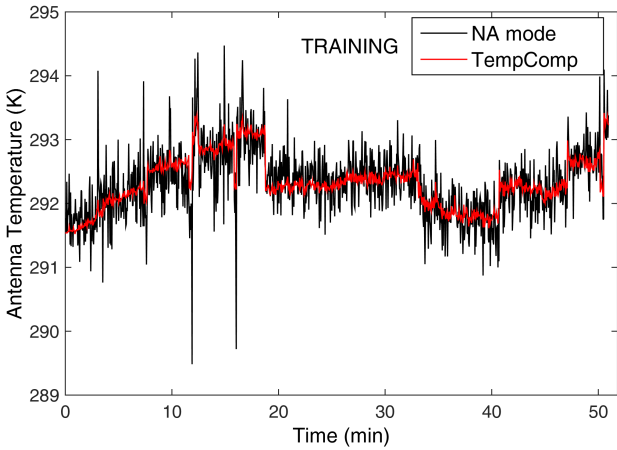


Fig. 6. Experiment 3 (February 23, 2017). Training set (first 50 min): time series of T_A in NA mode (black) and T_A estimated using the TempComp method (red).

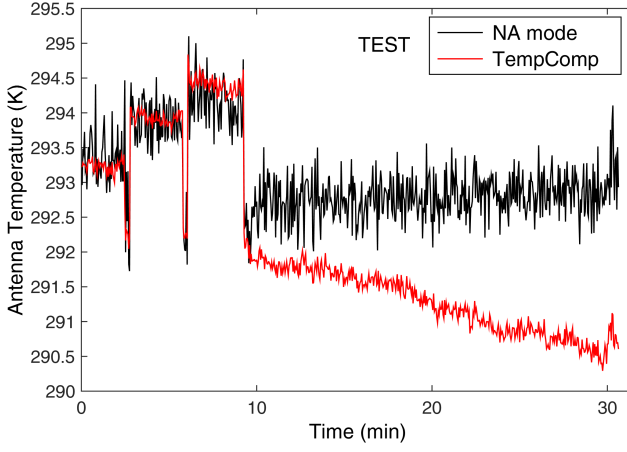


Fig. 7. Experiment 3 (February 23, 2017). Test set (last 30 min): time series of T_A in NA mode (black) and T_A estimated using the TempComp method (red).

$\Delta T = 0.4$ K in NA mode, crucial flaws occur that make the method unusable.

- 1) The calibration coefficients do not work well when applied to an independent data set with respect to the training one, even if the test set is temporally consecutive with the training set (the radiometer is not turned OFF); this drawback is particularly clear in Fig. 7.
- 2) The calibration coefficient computation should require the availability of a training set with known target temperatures (blackbody) at each data point or, at least, with T_A from an accurate and well calibrated radiometer; this is a critical point in the case of several experiments under different environmental conditions, since a new training phase should be performed every time.
- 3) The vulnerability of the calibration performance: the test-set RMSE can vary depending on the choice of the training-set length and thermal conditions, as we ascertained by processing the above experimental data.

V. DATA CALIBRATION PROCEDURE

As described in Section II, in MWR_NA operations, the NA mode continuously corrects for system gain fluctuations, while

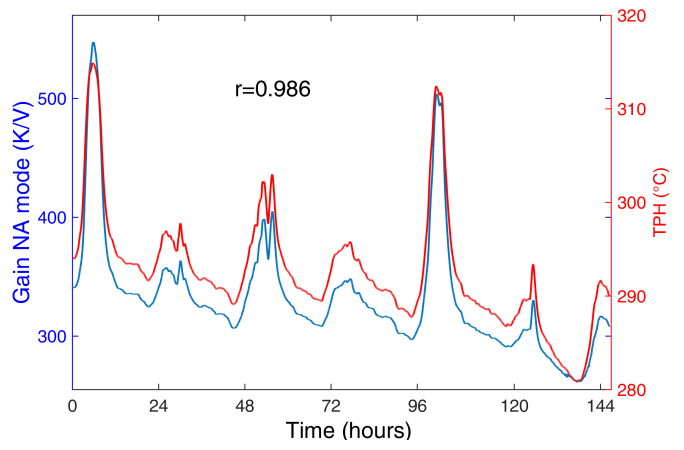


Fig. 8. Experiment 1. Time series of gain G in NA mode (blue) every 2.7τ s and of the corresponding radiometer internal physical temperature TPH (red). The Pearson correlation coefficient (r) is also reported.

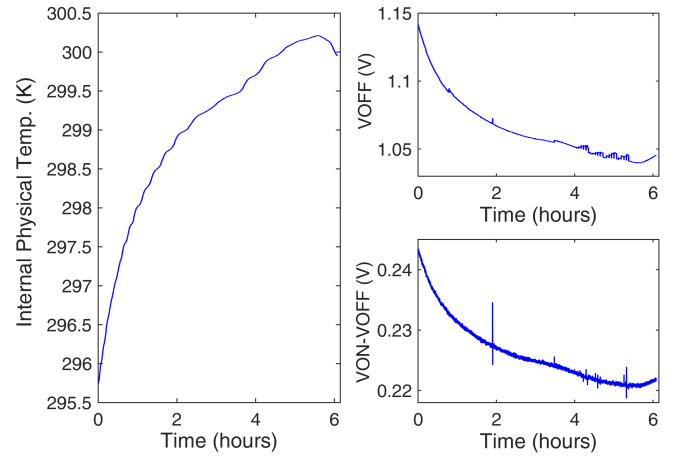


Fig. 9. Experiment 2. Time series of: TPH (radiometer internal physical temperature), V_{OFF} (voltage at the radiometer output when the noise source is switched OFF), $V_{ON} - V_{OFF}$ (the voltage difference determining gain G in NA mode).

the blackbody corrects for variations of the radiometric offset every 30 min for all the three experiments.

For experiment 1, Fig. 8 shows a clear influence of the internal physical temperature TPH on gain G in NA mode [$G = A/(V_{ON} - V_{OFF})$], as well as evident interior thermal excursions during the six days. The very high Pearson correlation coefficient ($r = 0.986$) between TPH and G , a measure of the linear correlation of the two variables, is also confirmed by experiment 2 ($r = 0.999$) and experiment 3 ($r = 0.985$). However, as shown in Section IV, such a very high r value does not guarantee good performance when applying least-squares estimation in the calibration phase.

Fig. 9 shows TPH , V_{OFF} , and $V_{ON} - V_{OFF}$ for experiment 2 and points out two main aspects.

- 1) The inverse correlation between the radiometer output voltages and TPH .
- 2) The “noise” of gain G in NA mode due to the voltage difference $V_{ON} - V_{OFF}$, determining also some “spikes” that are imperceptible in V_{OFF} . (It will also be evident in Section VI.)

To exploit the better radiometric resolution in TP mode, i.e., the reduced noise of the output signal, an efficient processing procedure for data calibration is proposed. Since the gain and offset stability both need the NA mechanism and the blackbody observations, we show how it is necessary to observe the scenario in NA mode only once every 30 min (not necessarily coincident with the blackbody observations).

In the following, the processing uses the same data set acquired in NA mode: therefore, the duty cycle is the same, i.e., V_{OFF} and V_{ON} are both observed for τ s.

As detailed in the following, the radiometric resolution improvement is achieved without time-averaging algorithms, the latter widely dealt with in [23]–[25].

This approach is suggested by the clear dependence of the gain G on the internal physical temperature (Fig. 8). The aim of the procedure is to estimate the gain in (3) at each measurement point adopting a linear dependence of G (NA mode) and T_{PH} extracted every 30 min. This time value has been chosen as a tradeoff between a longer time interval and a minimum decrease of the accuracy with respect to the standard calibration in NA mode. Therefore, the inspiring idea is to implement an adaptive temperature compensation between two successive (30 min away) NA injections.

Let us assume $G(h_i)$ the radiometric gain computed in NA mode at time h_i , and $G(h_{i+1})$ the gain acquired by the radiometer at time h_{i+1} after half an hour ($i = 1, \dots, N$, with N the number of “half an hour” for a specific radiometer experiment).

Therefore, the time interval $H_i = [h_i, h_{i+1}] = 30$ min. Inside H_i , the radiometer acquires a number of measurements k depending on the fixed acquisition time.

Let us model the value of G at time h_i as

$$G(h_i) = a_i T_{\text{PH}}(h_i) - c_i \quad (9)$$

and at time h_{i+1} as

$$G(h_{i+1}) = a_i T_{\text{PH}}(h_{i+1}) - c_i. \quad (10)$$

From these two measurements of G , it is possible to estimate the pair $(a_i$ and $c_i)$ for the time interval H_i , where a_i and c_i describe the slope and intercept of the linear relation between G and T_{PH} (i.e., the straight line passing for the two points in the T_{PH}, G plane) in such half an hour

$$a_i = [G(h_{i+1}) - G(h_i)]/[T_{\text{PH}}(h_{i+1}) - T_{\text{PH}}(h_i)] \quad (11)$$

$$c_i = a_i T_{\text{PH}}(h_i) - G(h_i). \quad (12)$$

Then, it is possible to estimate the gain $G_{\text{est},i}(k)$ at each single k point inside H_i as

$$G_{\text{est},i}(k) = a_i T_{\text{PH}}(k) - c_i. \quad (13)$$

This procedure is applied for each H_i , for $i = 1, \dots, N$.

Therefore, the antenna temperature T_A at each radiometer acquisition point, using the voltage output in TP mode, is computed as

$$T_A = G_{\text{est}} V_{\text{OFF}} - B. \quad (14)$$

In this way, the voltage output in NA mode is necessary only every half an hour, just like the B computation.

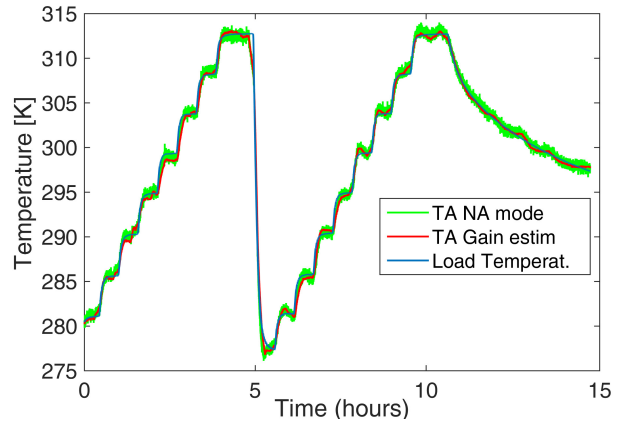


Fig. 10. Time series of physical temperatures of a WR75 load (blue) inserted in a climatic chamber and connected to the receiver input, the latter without thermal stabilization. Comparison with T_A measured by the radiometer in NA mode (green) and T_A estimated using G_{est} (red).

The accuracy and reliability of the proposed procedure are reported and discussed in Section VI.

VI. RESULTS AND DISCUSSION

Before to show the results for the three experiments, a rigorous test was carried out with the receiver input closed on a matched load in the WR75 waveguide acting as an ideal blackbody. The matched load was inserted into a climatic chamber and the receiver left at the ambient temperature without thermal stabilization. It can be considered a rigorous “early test” to assess the performance of the proposed calibration procedure. The chamber was programmed sweeping the load physical temperature between 275 and 315 K in 5-K steps [7]. The test, 15 h long and with $\tau = 1$ s, is reported in Fig. 10, where the load temperature (blue) is compared with the T_A measured by the radiometer in NA mode (green) and the T_A estimated using G_{est} (red). The RMSE between T_A and load physical temperatures is 0.63 K for both NA mode and G_{est} , showing the reliability of the proposed method in terms of both accuracy and improved radiometric resolution.

Concerning experiment 1, to compare the gain G computed in NA mode by (4) and the gain G_{est} estimated by (13), Fig. 11 reports the scatterplot of the two gains for all the data points collected every 2.7τ s. Figs. 12 and 13 show the scatterplots of T_{BB} and T_A computed with G and G_{est} , respectively. The T_{BB} standard deviation, which is equal to 5.25 K, can be assumed as an index of the variability of the parameter: a good accuracy of an estimation method is achieved when its RMSE is clearly below it, as in this case. Therefore, for experiment 1, in which the truth (T_{BB}) is available, the absolute accuracy of the standard calibration in NA mode is almost maintained for the new procedure.

The T_A time series in Figs. 14 and 15 describe the results for experiments 2 and 3, respectively. Table II reports the uncertainty in terms of RMSE and bias for the three experiments. Figs. 14 and 15 highlight the enhanced radiometric resolution of the new method (red curve) with respect to the one of the standard NA calibration (green curve).

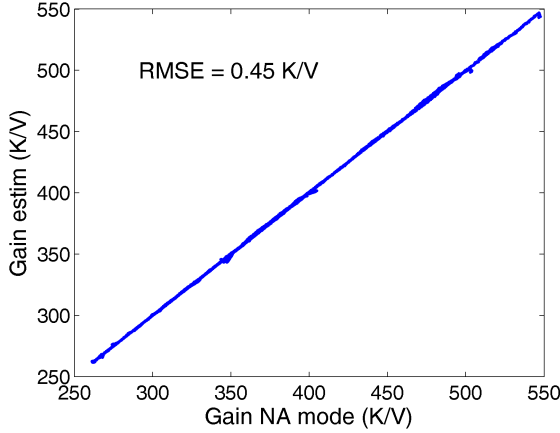


Fig. 11. Experiment 1. Scatterplot of gain G in NA mode and gain G_{est} estimated with the linear-temperature dependence (data points every 2.7 τ s). RMSE is reported.

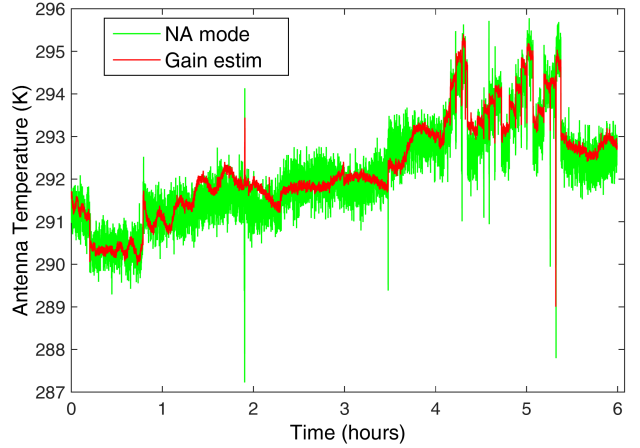


Fig. 14. Experiment 2. Time series of T_A measured in NA mode (green) and T_A computed using G_{est} (red).

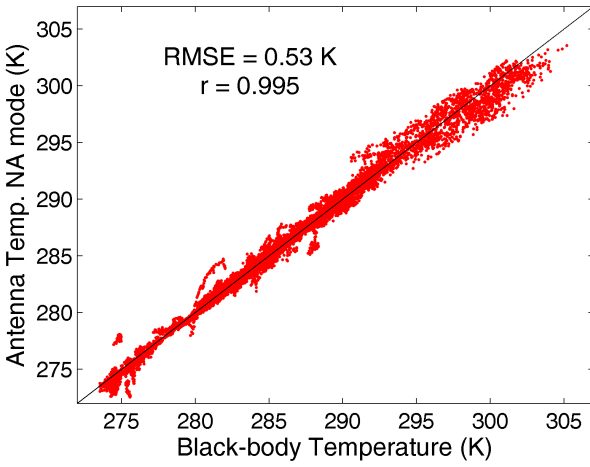


Fig. 12. Experiment 1. Scatterplot of T_{BB} and T_A measured in NA mode. RMSE and Pearson correlation coefficient (r) are reported. The T_{BB} variability (standard deviation) is 5.25 K.

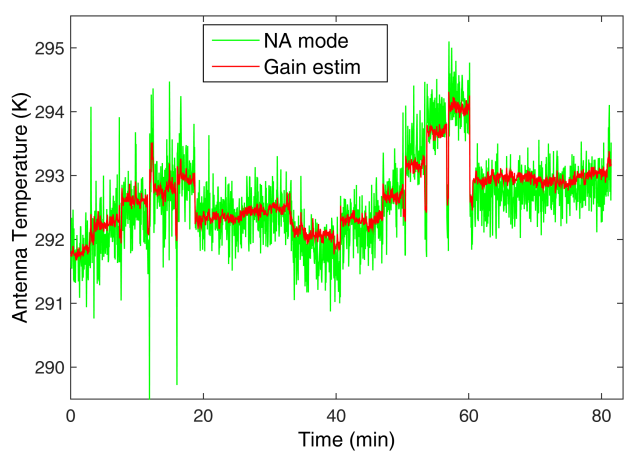


Fig. 15. Experiment 3. Time series of T_A measured in NA mode (green) and T_A computed using G_{est} (red).

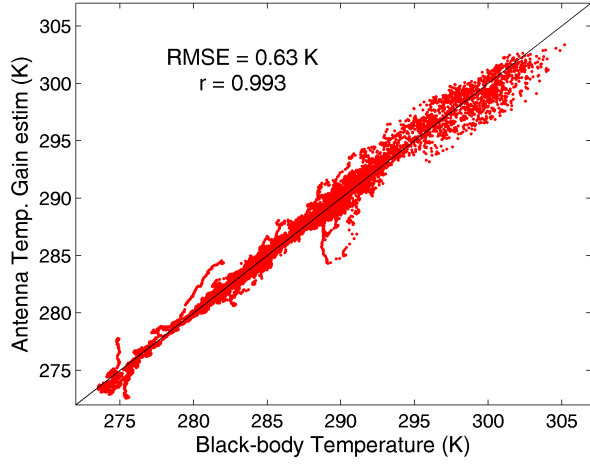


Fig. 13. Experiment 1. Scatterplot of T_{BB} and T_A computed using G_{est} . RMSE and Pearson correlation coefficient (r) are reported.

It is interesting to note some T_A spikes in NA mode, especially for experiments 2 and 3 where a smaller integration time is adopted, ascribed to $V_{\text{ON}} - V_{\text{OFF}}$ (Fig. 9), not present in the new estimation with G_{est} .

TABLE II
RMSE (K) AND BIAS (K) FOR THE THREE EXPERIMENTS
USING THE NEW METHOD FOR GAIN ESTIMATION

Comparison	RMSE	Bias
Experiment 1		
T_{BB} vs. T_A NA mode	0.53 K	0.01 K
T_{BB} vs. T_A Gain estim	0.63 K	0.01 K
Experiment 2		
T_A NA mode vs. T_A Gain estim	0.43 K	-0.14 K
Experiment 3		
T_A NA mode vs. T_A Gain estim	0.35 K	-0.07 K

Overall, a good agreement between T_A from (14) and T_A computed from (4) at each data point is found, confirming the accuracy preservation, as well as less-noisy observations, proving, in turn, the benefit of the proposed method to improve the radiometric resolution.

It is important to point out how the same procedure applied to the estimation of the radiometric offset B , i.e., using (9)–(13) with B instead of G , does not provide

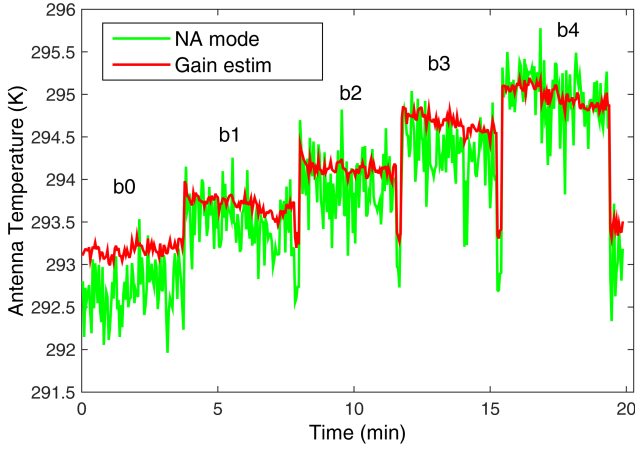


Fig. 16. Experiment 2. Time series of T_A in NA mode (green) and T_A using G_{estim} (red). bn corresponds to the number of bins of hot water placed in the antenna field of view.

a further accuracy improvement, but a slight worsening of RMSE (0.65 K) and bias (0.02 K) for experiment 1.

A. Advantages in Operative Scenarios

The two indoor experiments were carried out to evaluate the capability to detect temperature increments close to the radiometric resolution. To this purpose, we used warm targets with small filling factors inside the antenna field of view. The filling factor is the ratio of the solid angle subtended by the target over the antenna solid angle. In particular, the purpose was the detection of small radiation power increments due to targets placed sequentially in the antenna beam in order to demonstrate enabling counting capabilities of the radiometer. The targets were water (experiment 2) and oil (experiment 3) warmed up and poured in small styrofoam bins. Details of the experiments and a comparison with the correspondent electromagnetic model of the scenario are reported in [11]. With reference to Figs. 16 and 17, b0 corresponds to radiometer observations in the absence of bins (only the background is observed by the antenna), while bn ($n = 1, \dots, 4$) corresponds to n bins in the antenna footprint, with a filling factor of 1.4% for each bin.

The T_A trend in NA mode (green curve) suggests the incremental number of bins filled up by water or oil, even if the signal standard deviation may create ambiguity in target counting. Instead, the “less-noisy” observations computed using G_{estim} in TP mode (red curve) highlight a clearer difference of the bin contributions, without the ambiguous counting capability ascribed to the NA mode (see Appendix 1 for ΔT values). Taking into account the small filling factor of each bin (1.4%), the TP mode details an unambiguous T_A increment.

In Figs. 16 and 17, the sharp decrease of T_A during the positioning of different bins is due to the target handling phase (sample holder removal to fill up the successive bin).

In Fig. 16, a bias of 0.21 K is found: in any case the T_A with the new method is always inside the T_A fluctuations in NA mode, the latter having a standard deviation about 4–5 times greater (Table III).

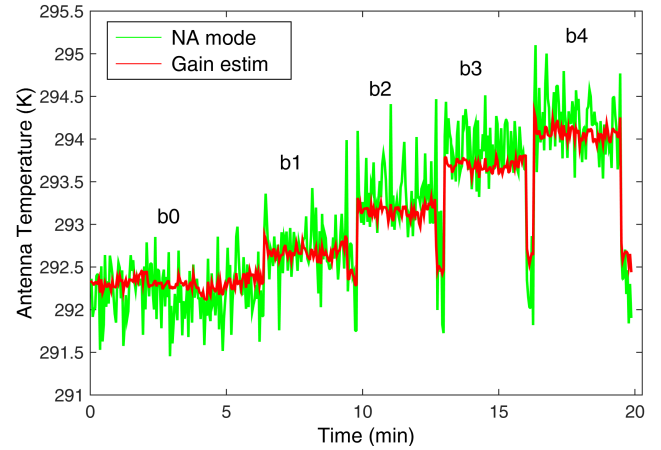


Fig. 17. Experiment 3. Time series of T_A in NA mode (green) and T_A using G_{estim} (red). bn corresponds to the number of bins of hot oil placed in antenna field of view.

TABLE III
EXPERIMENT 2: COMPARISON OF MEASURED AND THEORETICAL ΔT

Int. time τ	ΔT Measured	ΔT Theoretical
1 sec	0.37 K (NA mode)	0.44 K (NA mode)
1 sec	0.09 K (Gain estim)	0.07 K (TP mode)

Overall, the advantages of the proposed procedure for gain estimation with respect to the TempComp algorithm are as follows.

- 1) Greater accuracy.
- 2) The TempComp algorithm provides fixed calibration coefficients in the training phase that can be inadequate in the test phase: the proposed method provides two coefficients for the gain estimation that are updated every half an hour.
- 3) The proposed method does not require the availability of a training set with known target temperatures, but it is immediately applicable when the instrument starts the acquisitions, waiting for the first 30 min for the first pair of coefficients a_1 and c_1 .

Clearly, TempComp was conceived for a TP radiometer scheme and demonstrates the difficulty in developing an efficient calibration method without supplemental circuitry. From this standpoint, the NA system with periodical blackbody observations combines low complexity and cost with the efficiency of the data calibration procedure.

VII. CONCLUSION

The proposed gain estimation procedure, i.e., the combination of adaptive calibration/compensation data processing, provides better radiometric resolution and similar accuracy with respect to the standard NA calibration.

It can be easily implemented in the radiometer firmware, choosing whether to use it together with the standard NA mode (but with a longer measurement cycle), or programming the noise power injection every 30 min to take advantages of a shorter measurement cycle.

The benefit pointed out in the two indoor experiments can be certainly exploited in all the applications requiring a great radiometric resolution to detect small radiation power variations, both in outdoor and indoor environments regardless of the internal temperature drifts.

The development in the near future of system-on-chip microwave and millimeter-wave radiometers will further improve the sensing capability [26]–[29].

APPENDIX I RADIOMETRIC RESOLUTION

The radiometric resolution ΔT of the TP radiometer and of the NA one is reported the following the formulation in [1]. ΔT is the smallest change in T_A that can be detected by the radiometer output, determined by the standard deviation of the system input noise temperature.

For an ideal TP radiometer, i.e., accounting only for the noise fluctuations but without considering the receiver gain variations, the radiometric resolution is

$$\Delta T_{\text{ideal}} = \frac{T_{\text{SYS}}}{\sqrt{B\tau}} \quad (\text{A1})$$

where $T_{\text{SYS}} = T_A + T_R$ is the system input noise temperature, i.e., the sum of antenna (T_A) and receiver (T_R) input noise temperature, B is the receiver bandwidth (for MWR_NA is 100 MHz), and τ is the integration time.

Considering the gain variations, ΔT for a TP radiometer is

$$\Delta T = T_{\text{SYS}} \sqrt{\frac{1}{B\tau} + \left(\frac{\Delta G_R}{G_R} \right)^2} \quad (\text{A2})$$

where $\Delta G_R/G_R$ represents the normalized rms total fluctuations of the receiver component gain.

In the ΔT evaluation for the MWR_NA in TP mode, reported in Section II, a $\Delta G_R/G_R$ value of 1.35×10^{-4} was found.

Finally, the theoretical radiometric resolution for a NA TP radiometer is

$$\Delta T = 2\Delta T_{\text{ideal}} \left(1 + \frac{T_{\text{SYS}}}{T_{\text{ON}}} \right) \quad (\text{A3})$$

with T_{ON} the equivalent noise temperature injected by the noise source when it is ON. Details on T_{ON} value for the MWR_NA are reported in [7].

For experiments 2 and 3, T_R standard deviation (std) is below 0.5 K, T_A is in the range 290–295 K, and therefore these variations have no effect on ΔT . For experiment 1, T_R std is below 1.5 K, T_A is in the range 275–305 K, and ΔT variations in both TP and NA mode are negligible.

A comparison between measured and theoretical ΔT for experiment 2 is reported in Table III

If T_A is a few tens of degrees, as for clear sky observations, ΔT in NA mode is below 0.1 K, even if the ΔT value in TP mode is smaller. Since for the analyzed radiometer $T_{\text{sys}}/T_{\text{ON}}$ is greater than 1, ΔT in NA mode is always greater than 4 ΔT_{ideal} .

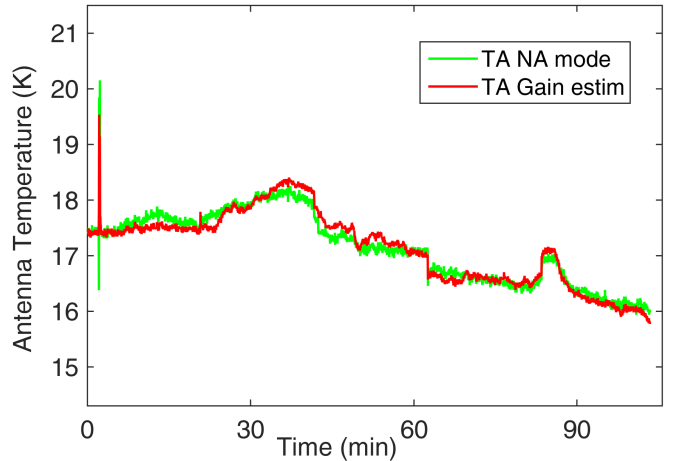


Fig. 18. Radiometer pointing the sky at zenith. Time series of T_A in NA mode (green) and T_A using G_{est} (red). The initial spike is due to a person within the antenna sidelobes.

APPENDIX II: ANTENNA TEMPERATURE AND RADIATION EFFICIENCY

The antenna temperature T'_A for an antenna with radiation efficiency η_R is

$$T'_A = \eta_R T_A + (1 - \eta_R) T_0 \quad (\text{A4})$$

where T_0 is the antenna physical temperature and T_A is the antenna noise temperature for a lossless antenna; η_R is equal to 1 for an ideal antenna. In this paper, the used aluminum horn antenna (15-dBi standard gain Waveline 7599, WR75 model) has a modeled $\eta_R = 0.977$. For experiments 1–3, the rms difference between T_A and T'_A (A4) is below 0.17 K, and no difference was found in the new procedure performance considering both uncorrected T'_A and corrected T_A .

Losses at input transmission lines are accounted in the radiometer calibration. The impedance matching of the receiver input featured an isolation of about 28 dB at 13 GHz [7].

A further test with the radiometer antenna pointing the sky (with the variable presence of not heavy clouds) at zenith was carried out to assess the proposed method performance with respect to the NA mode measurements. In this test, the radiometer observes very low antenna temperatures, corrected by (A4). Fig. 18 shows the time series of T_A measured by the radiometer in NA mode (green) and using G_{est} (red), exhibiting an RMSE of 0.15 K. As described in Appendix I, a considerable improvement of ΔT in NA mode is observed, even if ΔT in TP mode is slightly better.

Even though the instrument was not well characterized for the reference scenario with very low brightness temperatures, the results confirm that the T_A with the proposed gain estimation follows the T_A in the NA mode. Also, the expected clear improvement of ΔT in NA mode points out that the proposed procedure is particularly useful for the measurement of T_A in the range of experiments 1–3 rather than for very low T_A .

ACKNOWLEDGMENT

The authors would like to thank R. Rossi and Dr. R. V. Gatti for the horn antenna characterization.

REFERENCES

- [1] F. T. Ulaby, R. K. Moore, and A. K. Fung, *Microwave Remote Sensing*. Norwood, MA, USA: Artech House, 1981.
- [2] J. Querol, J. M. Tarongí, G. Forte, J. J. Gómez, and A. Camps, “MERITXELL: The multifrequency experimental radiometer with interference tracking for experiments over land and littoral—Instrument description, calibration and performance,” *Sensors*, vol. 17, no. 5, p. 1081, 2017.
- [3] K. Saleh *et al.*, “Estimates of surface soil moisture under grass covers using L-band radiometry,” *Remote Sens. Environ.*, vol. 109, no. 1, pp. 42–53, 2007.
- [4] Y. Sawada, H. Tsutsui, T. Koike, M. Rasmy, R. Seto, and H. Fujii, “A field verification of an algorithm for retrieving vegetation water content from passive microwave observations,” *IEEE Trans. Geosci. Remote Sens.*, vol. 54, no. 4, pp. 2082–2095, Apr. 2016.
- [5] A. V. Bosisio and C. Capsoni, “Effectiveness of brightness temperature ratios as indicators of atmospheric path conditions,” in *Microwave Radiometry and Remote Sensing of the Environment*, D. Solimini, Ed. Utrecht, The Netherlands: VSP, 1995, pp. 129–138.
- [6] F. S. Marzano, E. Fionda, P. Ciotti, and A. Martellucci, “Ground-based multifrequency microwave radiometry for rainfall remote sensing,” *IEEE Trans. Geosci. Remote Sens.*, vol. 40, no. 4, pp. 742–759, Apr. 2002.
- [7] F. Alimenti *et al.*, “A low-cost microwave radiometer for the detection of fire in forest environments,” *IEEE Trans. Geosci. Remote Sens.*, vol. 46, no. 9, pp. 2632–2643, Sep. 2008.
- [8] G. Tasselli, F. Alimenti, S. Bonafoni, P. Basili, and L. Roselli, “Fire detection by microwave radiometric sensors: Modeling a scenario in the presence of obstacles,” *IEEE Trans. Geosci. Remote Sens.*, vol. 48, no. 1, pp. 314–324, Jan. 2010.
- [9] J. T. Johnson, H. Kim, D. R. Wiggins, and Y. Cheon, “Subsurface object sensing with a multifrequency microwave radiometer,” *IEEE Trans. Geosci. Remote Sens.*, vol. 40, no. 12, pp. 2719–2726, Dec. 2002.
- [10] F. Jonard, L. Weihermüller, M. Schwank, K. Z. Jadoon, H. Vereecken, and S. Lambot, “Estimation of hydraulic properties of a sandy soil using ground-based active and passive microwave remote sensing,” *IEEE Trans. Geosci. Remote Sens.*, vol. 53, no. 6, pp. 3095–3109, Jun. 2015.
- [11] F. Alimenti, S. Bonafoni, and L. Roselli, “A novel sensor based on a single-pixel microwave radiometer for warm object counting: Concept validation and IoT perspectives,” *Sensors*, vol. 17, no. 6, p. 1388, 2017.
- [12] J. T. Johnson, M. A. Demir, and N. Majurec, “Through-wall sensing with multifrequency microwave radiometry: A proof-of-concept demonstration,” *IEEE Trans. Geosci. Remote Sens.*, vol. 47, no. 5, pp. 1281–1288, May 2009.
- [13] N. Skou, *Microwave Radiometer Systems: Design and Analysis*. Norwood, MA, USA: Artech House, 1989.
- [14] R. Dicke, “The measurement of thermal radiation at microwave frequencies,” *Rev. Sci. Instrum.*, vol. 17, no. 7, pp. 268–275, 1946.
- [15] *Microwave Radiometer (MWR) Handbook—ARM Climate Research Facility*. Accessed: Sep. 7, 2017. [Online]. Available: www.arm.gov/publications/tech_reports/handbooks/mwr_handbook.pdf
- [16] K. Al-Ansari, P. Garcia, J. M. Riera, A. Benaroch, D. Fernandez, and L. Fernandez, “Calibration procedure of a microwave total-power radiometer,” *IEEE Microw. Wireless Compon. Lett.*, vol. 12, no. 3, pp. 93–95, Mar. 2002.
- [17] D. A. Thompson, R. L. Rogers, and J. H. Davis, “Temperature compensation of total power radiometers,” *IEEE Trans. Microw. Theory Techn.*, vol. 51, no. 10, pp. 2073–2078, Oct. 2003.
- [18] C.-S. Chae, J.-H. Kwon, and Y.-H. Kim, “A study of compensation for temporal and spatial physical temperature variation in total power radiometers,” *IEEE Sensors J.*, vol. 12, no. 6, pp. 2306–2312, Jun. 2012.
- [19] F. Alimenti, G. Tasselli, C. Botteron, P.-A. Farine, and C. Enz, “Avalanche microwave noise sources in commercial 90-nm CMOS technology,” *IEEE Trans. Microw. Theory Techn.*, vol. 64, no. 5, pp. 1409–1418, May 2016.
- [20] P. Béland, S. Labonte, L. Roy, and M. Stubbs, “A novel on-wafer resistive noise source,” *IEEE Microw. Guided Wave Lett.*, vol. 9, no. 6, pp. 227–229, Jun. 1999.
- [21] L. P. Dunleavy, J. Randa, D. K. Walker, R. Billinger, and J. Rice, “Characterization and applications of on-wafer diode noise sources,” *IEEE Trans. Microw. Theory Techn.*, vol. 46, no. 12, pp. 2620–2628, Dec. 1998.
- [22] P. F. Goldsmith, *Quasioptical Systems: Gaussian Beam Quasioptical Propagation and Applications*. Piscataway, NJ, USA: IEEE Press, 1998.
- [23] J. C. Bremer, “Improvement of scanning radiometer performance by digital reference averaging,” *IEEE Trans. Instrum. Meas.*, vol. IM-28, no. 1, pp. 46–54, Mar. 1979.
- [24] P. Racette, R. F. Adler, J. R. Wang, A. J. Gasiewski, and D. S. Zacharias, “An airborne millimeter-wave imaging radiometer for cloud, precipitation, and atmospheric water vapor studies,” *J. Atmos. Ocean. Technol.*, vol. 13, no. 3, pp. 610–619, 1996.
- [25] P. Racette, M. Triesky, and D. Jones, “A multi-channel microwave radiometer uses reference averaging for calibration: Precision approaches that of a total power radiometer,” in *Proc. IGARSS*, vol. 3. Seattle, WA, USA, Jul. 1998, pp. 1695–1697.
- [26] J. W. May and G. M. Rebeiz, “Design and characterization of W-band SiGe RFICs for passive millimeter-wave imaging,” *IEEE Trans. Microw. Theory Techn.*, vol. 58, no. 5, pp. 1420–1430, May 2010.
- [27] A. Tomkins, P. Garcia, and S. P. Voinigescu, “A passive W-band imaging receiver in 65-nm bulk CMOS,” *IEEE J. Solid-State Circuits*, vol. 45, no. 10, pp. 1981–1991, Oct. 2010.
- [28] J. J. Lynch *et al.*, “Passive millimeter-wave imaging module with preamplified zero-bias detection,” *IEEE Trans. Microw. Theory Techn.*, vol. 56, no. 7, pp. 1592–1600, Jul. 2008.
- [29] F. Alimenti *et al.*, “System-on-chip microwave radiometer for thermal remote sensing and its application to the forest fire detection,” in *Proc. ICECS*, St. Julien’s, Malta, Aug./Sep. 2008, pp. 1265–1268.



S. Bonafoni (M’12) received the Laurea (*cum laude*) and the Ph.D. degrees in electronic engineering from the University of Perugia, Perugia, Italy, in 1997 and 2000, respectively.

Since 2005, she has been with the Department of Engineering, University of Perugia, where she teaches “remote sensing.” Her research interests include retrieval of geophysical parameters from ground-based and space-based sensors (by microwave and infrared radiometry and by GPS), microwave propagation studies in the atmosphere (models and applications), and analysis of the urban heat island by satellite thermal remote sensing.



F. Alimenti (S’91–A’97–M’06–SM’09) received the Laurea and Ph.D. degrees in electronic engineering from the University of Perugia, Perugia, Italy, in 1993 and 1997, respectively.

From 2011 to 2014, he was the Scientific Coordinator of the ENIAC ARTEMOS Project. In 2014, he joined the École Polytechnique Fédérale de Lausanne, Lausanne, Switzerland, as a Visiting Professor. In 1996, he joined the Technical University of Munich, Munich, Germany, as a Visiting Scientist. Since 2001, he has been with the Department of Engineering, University of Perugia, where he teaches “microwave electronics.” He has an *h*-index of 18 in Google Scholar. His research interests include microwave integrated circuit design and electronics on cellulose.

Dr. Alimenti was a recipient of the URSI Young Scientist Award in 1996 and the IET Premium (Best Paper) Award in 2013. He was the TPC Chair of the IEEE Wireless Power Transfer Conference in 2013.



L. Roselli (M’92–SM’01–F’18) joined the University of Perugia, Perugia, Italy, in 1991. In 2000, he founded the spin-off WiS Srl. He has been involved in electronic technologies for Internet of Things for the past seven years. He is currently a Qualified Full Professor with the University of Perugia, where he teaches applied electronics and coordinates the HFE-Laboratory. He has authored over 300 contributions (H-i 27, i10 67, over 2500 citations—Scholar) and the book *Green RFID Systems* (Cambridge University Press). His research interests include HF electronic systems with a special attention to RFID, new materials, wireless power transfer, and electronic technologies for Internet of Things.

Dr. Roselli was a member of the Board of Directors of ART srl from 2008 to 2012. He is currently a member of the list of experts of the Italian Ministry of Research, a Past Chair of the IEEE Technical Committees MTT24-RFID, a Vice-Chair of 25-RF Nanotechnologies, a member of the MTT-26-Wireless Power Transfer, a Past Member of the ERC Panel PE7, H2020 evaluator, a member of the Advisory Committee of the IEEE-WPTC, and a Chairman of the SC-32 of IMS. He is the Co-Chair of the IEEE Wireless Sensor Network Conference. He organized the VII Computational Electromagnetic Time Domain in 2007 and the first IEEE-Wireless Power Transfer Conference in 2013. He is an Associate Editor of *IEEE Microwave Magazine*. He is also involved in the boards of several international conferences.